Nanoscale Horizons

ROYAL SOCIETY OF CHEMISTRY

COMMUNICATION

View Article Online
View Journal | View Issue

Cite this: *Nanoscale Horiz.*, 2023, **8**, 776

Received 20th February 2023,
Accepted 8th March 2023

DOI: 10.1039/d3nh00063j

rsc.li/nanoscale-horizons

Simple engineering of hybrid cellulose nanocrystal–gold nanoparticles results in a functional glyconanomaterial with biomolecular recognition properties†

Giacomo Biagiotti,‡[a] Gianluca Toniolo,‡[ab] Martin Albino,[ac] Mirko Severi,[a] Patrizia Andreozzi,[a] Marcello Marelli,[d] Hana Kokot,[e] Giancarlo Tria,[a] Annalisa Guerri,[a] Claudio Sangregorio,[c] Javier Rojo,[f] Debora Berti,[ag] Marco Marradi,[a] Stefano Cicchi,[ab] Iztok Urbančič,[e] Yvette van Kooyk,[h] Fabrizio Chiodo *[hi] and Barbara Richichi *[ab]

Cellulose nanocrystal and gold nanoparticles are assembled, in a unique way, to yield a novel modular glyconanomaterial whose surface is then easily engineered with one or two different headgroups, by exploiting a robust click chemistry route. We demonstrate the potential of this approach by conjugating monosaccharide headgroups to the glyconanomaterial and show that the sugars retain their binding capability to C-type lectin receptors, as also directly visualized by cryo-TEM.

Cellulose nanocrystal (CNC) is a low-cost functional material that can be easily prepared by controlled acidic hydrolysis from several renewable sources.[1] Owing to its distinctive biocompatibility, biodegradability and excellent chemical stability, CNC has emerged as one of the most appealing natural biopolymeric scaffolds. As such, it has the potential to be exploited as a 'magic bullet' for nanomedicine.[2] Small spindle-like size, stiff chain architecture, and large surface area (250–500 $m^2\ g^{-1}$), are unique features that allow for the preparation of advanced nanomaterials for many applicative areas, including material and life sciences.[3] Concerning biological systems, the known protein-repellent properties of polysaccharide-based nanomaterials make CNC a suitable nanocarrier for the development of therapeutics, resulting in prolonged circulation in the bloodstream, and delayed opsonization and removal by immune cells.[4a,b] In addition, its rod-shaped morphology and surface chemistry significantly affect CNC fate. Interestingly, CNC exhibits slower rates of renal clearance, and from the perspective of drug delivery, pristine nanocrystals demonstrated low unspecific uptake in several cell types.[2a,4a] Furthermore, the hydroxyl groups on the glucose residues enable easy functionalization and bioconjugation[5] of the CNC surface with specific

New concepts

In this work, sulfated cellulose nanocrystal (CNC) and gold nanoparticles (AuNPs) are assembled in a unique and straightforward way providing a new modular and functional glyconanomaterial (named CNC–Au–LA). Our CNC–AuNPs is a glyconanomaterial that provides a conceptual advance in the field: it combines the complementary physiochemical properties of AuNPs and polysaccharide-based nanomaterials along with preserving the main composition and structure of the pristine CNC. Owing to its unique structure, our CNC–AuNPs surface is easily engineered with one or two different headgroups, by exploiting a robust click chemistry route, under strictly controlled reaction conditions. The grafting of C-type lectin receptor (CLR)-targeting monosaccharides makes our glyconanomaterial a powerful tool for a direct visualization of the sugar headgroup–lectin interactions by cryo-transmission electron microscopy. We believe that our findings represent an important step that opens up new roads for further investigations of this kind of hybrid glyconanomaterials as the "next generation" of multifunctional biocompatible nanotools.

[a] *Department of Chemistry "Ugo Schiff", University of Firenze, Via della Lastruccia 13, 50019 Sesto Fiorentino (Firenze), Italy. E-mail: barbara.richichi@unifi.it*
[b] *Consorzio Interuniversitario Nazionale per la Scienza e Tecnologia dei Materiali (INSTM), 50121 Firenze, Italy*
[c] *ICCOM CNR via Madonna del Piano 10, 50019 Sesto Fiorentino (Firenze), Italy*
[d] *Istituto di Scienze e Tecnologie Chimiche "Giulio Natta", SCITEC-CNR, Via G. Fantoli 16/15, 20138, Milano, Italy*
[e] *Laboratory of Biophysics, Condensed Matter Physics Department, Jožef Stefan Institute, Jamova c. 39, 1000, Ljubljana, Slovenia*
[f] *Glycosystems Laboratory, Instituto de Investigaciones Químicas (IIQ), CSIC - Universidad de Sevilla, Av. Américo Vespucio 49, Seville, 41092, Spain*
[g] *Italian Center for Colloid and Surface Science (CSGI), 50019 Sesto Fiorentino (Firenze), Italy*
[h] *Amsterdam UMC, Vrije Universiteit Amsterdam, Department of Molecular Cell Biology and Immunology, Amsterdam Infection and Immunity Institute, Amsterdam, The Netherlands. E-mail: f.chiodo@amsterdamumc.nl*
[i] *Institute of Biomolecular Chemistry, National Research Council (CNR), Pozzuoli, Napoli, Italy*

† Electronic supplementary information (ESI) available: Synthetic procedures, protocols for the ELISA solid-phase assay, X-ray diffraction (XRD), microscopy measurements, and the turbidimetry assay, and NMR spectra of the CNC conjugates. See DOI: https://doi.org/10.1039/d3nh00063j

‡ G.B. and G.T. contributed equally.

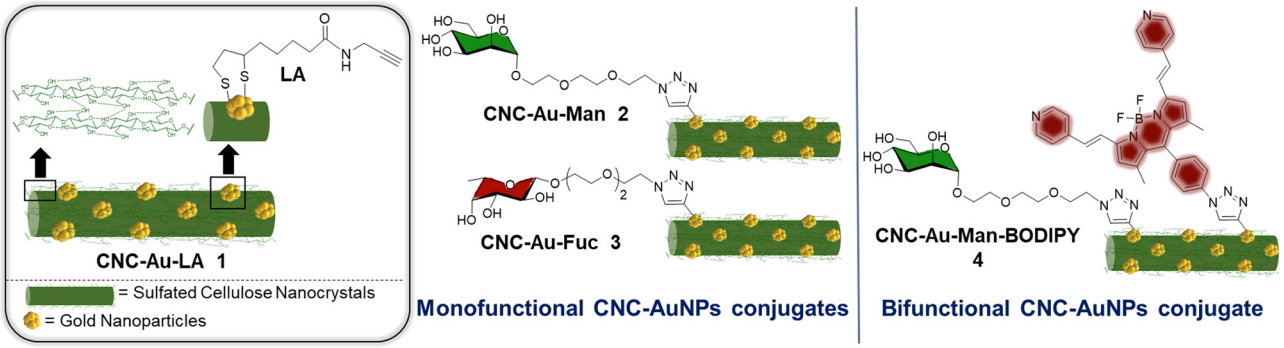

Fig. 1 Schematic representation of the CNC–Au–LA **1**, the monofunctional conjugates CNC–Au–Man **2** and CNC–Au–Fuc **3**, and the bifunctional conjugate CNC–Au–Man–BODIPY **4**.

bioactive molecules that allow targeting to disease sites.[2b,c] The stiff chain architecture makes CNC an excellent platform for the fabrication of metal nanohybrids.[1b,6] Among them, CNC–gold nanoparticles (CNC–AuNPs) composites are attractive hybrid nanomaterials with unique catalytic and sensing properties.[7] Protocols for CNC–AuNPs preparation usually employ chemical modifications of the CNC surface with molecules that work as reducing agents or stabilizers of gold ion precursors.[7] Unfortunately, the pre-treatment steps result in significant structural modifications of the CNC composition and surface chemistry that, in turn, may significantly impact the physicochemical properties and nano–bio interactions of the pristine CNC.[8a,b] Therefore, identifying straightforward methodologies that enable easy access to CNC–AuNPs nanohybrids where the properties of both components are preserved is highly demanding.[9]

In this context, we report here on the synthesis of an easily affordable and modular CNC–AuNPs hybrid glyconanomaterial, CNC–Au–LA **1** (Fig. 1). This composite was prepared by exploiting a novel and straightforward one-step protocol that combines, in a unique way, the polysaccharide-based glyconanomaterial with AuNPs, preserving the main composition and structure of the sulfated pristine CNC scaffold. Moreover, this approach lends itself to straightforward post-functionalization with headgroups and therefore paves the way to a library of modular glyconanomaterials with the same biocompatible scaffold.

Utilizing this strategy, small AuNPs bearing a lipoamide (LA) spacer with a terminal chemical reporter (alkyne residue) were stably embedded into the CNC matrix (Fig. 1). Alkyne residues were harnessed for the covalent conjugation by a controlled Cu(I)-catalyzed azide–alkyne cycloaddition (CuAAC) of one or two structurally different functionalities. C-type lectin receptors (CLRs) targeting moieties (*i.e.* mannose and fucose for CNC–Au–Man **2** and CNC–Au–Fuc **3** respectively, Fig. 1) and a BODIPY-like fluorescent dye (CNC–Au–Man–BODIPY **4**, Fig. 1) were included thus affording the mono- and bifunctional conjugates **2–4**. Notably, CNC glyconanohybrids **2** and **3** bind to CLRs (*i.e.* Langerin and DC-SIGN)[10] *via* the monosaccharide residues installed on the gold surface. Then, utilizing cryo-transmission electron microscopy (cryo-TEM), we were able to visualize sugar headgroup-lectin interactions by cryogenic microscopy.

At first, AuNPs were prepared *in situ* in a one-step protocol using commercially available sulfated CNC as the template (ESI†), Au(III) salts (tetrachloroauric acid, $HAuCl_4$) as precursors of AuNPs and the α-lipoamide (LA) spacer **5** (Scheme 1A) as a ligand to ensure the formation of Au–S bonds.[11] The use of $NaBH_4$ as reducing agent allowed for the quick formation of Au

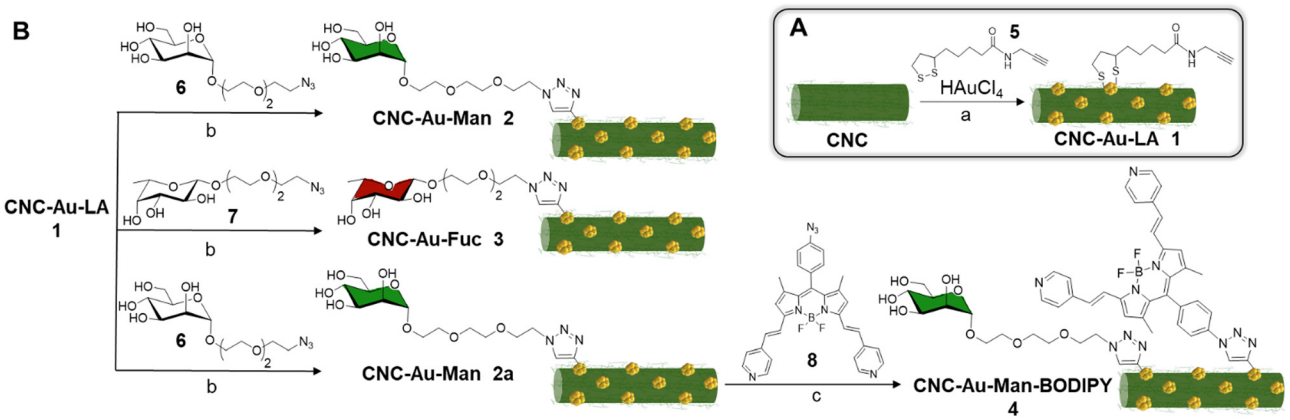

Scheme 1 A. Synthesis of CNC–Au–LA **1.** B. Synthesis of CNC–Au–Man **2**, CNC–Au–Fuc **3**, and CNC–Au–Man–BODIPY **4**. Reaction conditions: (a) $NaBH_4$, MeOH : H_2O (9 : 1), rt, 2 h; (b) $CuSO_4$, sodium ascorbate, H_2O, rt, 12 h; (c) $CuSO_4$, sodium ascorbate, DMF, rt, 12 h.

nanoclusters that undergo *in situ* stabilization by the LA derivative **5**. The use of a methanol : water mixture (9 : 1 ratio) was crucial for installing the LA spacer **5** on the Au surface *in situ*, thus ensuring the dispersibility of all the reaction components. The resulting CNC–Au–LA **1** was easily purified by dialysis, and then fully characterized through a set of complementary techniques.

Transmission electron microscopy (TEM) showed small AuNPs (mean Au core diameter around 4.0 nm) with a narrow size distribution, as more than 80% of the particles were less than 5 nm (ESI,† Fig. S1). These particles were stably embedded into the CNC matrix, thereby avoiding CNC additional derivatization, usually approached to obtain homogeneous nanoparticle distributions.[7] As expected for small-sized AuNPs,[12] UV-Vis adsorption spectra (ESI,† Fig. S2) of both the reaction mixture over time and the final CNC–Au–LA **1** did not show a well-defined plasmon absorption maximum[12] (at around 520 nm) typical of AuNPs with larger diameters. The atomic percentage of Au in the CNC–Au–LA **1** was estimated by inductively coupled plasma atomic emission spectroscopy (ICP-AES) and it consisted of 9.2% w/w (92 μg mg^{-1}). This implies that more than 90% of the starting Au salt (ESI†) was converted into AuNPs, thus providing quantitative evidence of Au recovery. Additionally, the loading of the spacer **5** was assessed by elemental analysis to be roughly 17% w/w (0.072 mmol of **5** over 100 mg of **1**, based on nitrogen content: ESI,† Table S1).

The presence of the LA residues on the CNC surface was also confirmed by the ^{1}H NMR spectrum of a DMSO-d6 dispersion of CNC–Au–LA **1** (ESI,† Fig. S3). Then, scanning transmission electron microscopy/energy dispersive X-ray (STEM-EDX) analysis of CNC–Au–LA **1** confirmed the co-presence of Au and S (ESI,† Fig. S4) due to the LA spacer attached to the AuNPs surface through the terminal thiol groups. The X-ray diffraction (XRD) patterns of the CNC–Au–LA **1** (ESI,† Fig. S5) exposed two different crystalline phases that were compatible with the cubic structure characteristic of Au and the monoclinic structure characteristic of cellulose. All the peaks matched for the position and intensity of the reference patterns (*i.e.* JCPDS 00-066-0091 (gold) and JCPDS 00-056-1718 (cellulose Iβ)) and the lattice parameters (a = 4.0791(7) Å, Au; a = 7.8613(1) Å, b = 8.0500(3) Å, c = 10.4790(6) Å, β = 92.9533(9)°, cellulose Iβ) were close to those expected for bulk Au (a = 4.0778 Å) and cellulose Iβ (a = 7.784 Å, b = 8.201 Å, c = 10.38 Å, β = 96.5°), respectively, confirming that the samples consisted of cellulose nanorods coated with AuNPs. The Au crystallite diameter (d_{XRD} = 3.9(2) nm), obtained by Scherrer analysis, is comparable to the size obtained with TEM measurements, suggesting that the AuNPs may be considered single crystals with a high degree of crystallinity. Furthermore, XRD data, compared with those obtained by TEM analysis, provided further evidence for the presence of a typical semicrystalline cellulose structure, with an average crystallite size of 4.8(1) nm. Finally, the ζ-potential of CNC–Au–LA **1** was −41 ± 1 mV, indicating that the synthetic process does not significantly affect the surface charge of the sulfated pristine CNC (*i.e.* ζ = −39 ± 2 mV).

Glycosides **6** and **7** (Scheme 1B), respectively, a D-mannose derivative (Man, compound **6**, Scheme 1B) and a L-fucose derivative (Fuc, compound **7**, Scheme 1B) bearing a PEGylated linker at the anomeric position, were prepared according to a previously reported protocol.[13] The terminal azide groups of **6** and **7** were reacted with the alkyne residues on the CNC–Au–LA **1** surface using a CuAAC in H_2O using a 2 : 1 glycosides to LA ratio. The loading of the sugar headgroups was calculated by elemental analyses based on the nitrogen content of **2** and **3** compared with the precursor CNC–Au–LA **1** (1.02% w/w in **1** *vs.* 1.60% w/w in **2** *vs.* 1.58% w/w in **3**, Table S1, ESI†). In particular, elemental analyses showed a loading of the saccharides **6** and **7**, respectively, of 5.21% w/w (*i.e.* 0.027 mmol of Man over 100 mg of **2**, Table S1, ESI†) for CNC–Au–Man **2** and 4.25% w/w (*i.e.* 0.039 mmol of Fuc over 100 mg of **3**, Table S1, ESI†) for CNC–Au–Fuc **3**. The presence of the sugar headgroups on the CNC surface was confirmed by the ^{1}H NMR spectrum of **2** and **3** that provided signals in the range of 3.8–4.8 ppm that can be attributed to the monosaccharides **6** and **7** (ESI,† Fig. S6 and S7).

The synthesis of the bifunctional conjugate **4** was performed to demonstrate that this approach allows for the simultaneous covalent grafting of different headgroups on the glyconanomaterial surface by fine-tuning the equivalents of the azide-bearing reagents employed in an iterative step-by-step conjugation route (Scheme 1B). In particular, the mannose CNC-conjugate **2** was selected as the model nanomaterial. At first, a CuAAC using a mannoside **6** : LA ratio of 0.5 : 1 was performed in the same experimental conditions reported above. Then, the resulting CNC–Au–Man **2a** (3.55% w/w loading of **6**, ESI,† Table S1) was further conjugated to the BODIPY **8**[14] in DMF (Scheme 1B) affording the CNC–Au–Man–BODIPY **4**. The grafting of the CNC–AuNPs surface was controlled step-by-step using elemental analysis (ESI,† Table S1) and UV-vis spectroscopy. The loading of the BODIPY **8** on the surface of **5** was estimated by UV-vis spectroscopy (λ_{max} = 630 nm) using the molar extinction coefficient of BODIPY **8**[14] in DMSO and was found to be 0.46% w/w (ESI,† Fig. S8) according to the boron content assessed by ICP-AES analysis (ESI,† Table S1). Furthermore, excitation with UV-light (λ_{max} = 380 nm or 580 nm) resulted in a fluorescence emission peak at λ = 635 nm (ESI,† Fig. S8), whereas no emission of the precursor CNC–Au–Man **2a** was observed (data not shown). In addition, the CNC–Au–Man–BODIPY **4** was nicely detected under the laser-scanning confocal microscope (ESI,† Fig. S9A). The shortened fluorescence lifetime observed for **4** compared to BODIPY **8** (2.0–2.7 ns and 3.2 ns, respectively; ESI,† Fig. S9B and C) can be related to the plasmonic effects of the nearby AuNPs or self-quenching of the neighboring dyes on the surface of CNC. Of note, the photo-stability of the CNC–Au–Man–BODIPY **4** was assessed on LA-4 murine lung epithelial cells using the commercially available Atto647N-DPPE (ESI†) as a control. Data showed that the CNC–Au–Man–BODIPY **4** is very photo-stable under continuous confocal recordings (ESI,† Fig. S10), indicating its potential for further long-term imaging experiments.

Then, we performed agglutination studies to prove the persistence of bioactivity of the sugar headgroups on the CNC–AuNPs conjugates and, specifically, if the arrangement of the sugar headgroups allowed for proper recognition by lectins' carbohydrate binding domain.[15] We initially selected

the CNC–Au–Man **2** as our CNC glycoconjugate and Concanavalin A (ConA),[16] a plant lectin broadly used for investigating the multivalent binding of glyco-constructs,[17] as a model lectin. ConA is a tetramer at neutral pH and it has a high binding affinity with D-mannose and D-glucose (and glycopolymers with α-D-glucopyranosyl subunits).[17a,18] We thus expect aggregation of ConA with CNC–Au–Man **2** driven by molecular recognition of the mannose headgroups of **2**. With this in mind, CNC–Au–LA **1** was used as a control. At first, the colloidal stability of **2** (ESI,† Fig. S11) in 2-(4-(2-hydroxyethyl)piperazin-1-yl)ethane-1-sulfonic acid (HEPES) buffer was monitored at room temperature over time (0–90 min). Then, we studied the interaction of **2** (0.01% w/w) with increasing concentrations of ConA (0–11.3 μM) (ESI,† Fig. S12), by measuring the change in absorption (λ = 490 nm) after 60 min of incubation.[19] ConA concentration-dependent agglutination was observed as indicated by turbidity measurements (ESI,† Fig. S12). Agglutination was also monitored over time by measuring the absorbance changes, upon addition of a suspension of **2** (0.01% w/w) to a fixed concentration of ConA (10 μM in HEPES buffer, ESI†). The data obtained (ESI,† Fig. S11) indicated that the turbidity of the solution increased over time. No change in the absorption was observed by titration of CNC–Au–LA **1** with ConA (ESI,† Fig. S13), hereby confirming that the aggregation was a consequence of the recognition of the mannose headgroups on the surface of **2** by the lectin. These results prove that the engineering of the CNC–Au–LA surface ensures an arrangement of the mannose headgroups that permits the specific recognition of the monosaccharide residues by the ConA.

On this basis, the binding of the CNC–AuNPs glycoconjugates to the calcium/magnesium-dependent C-type lectin receptors (CLRs) DC-SIGN and langerin (as members of the group 2 of CLRs) was further studied by an ELISA-based solid phase assay (ESI†).[20] Fig. 2 shows the binding of the tested chimera lectins[21,22] to glyconanomaterials-coated ELISA plates. Mannan and polyacrylic acid-Lewis^X (PAA-Le^x) were used as a positive control. In these experimental conditions, the langerin lectin showed a different binding on the CNC–Au–Man **2** than the CNC–Au–Fuc **3** (Fig. 2), in agreement with the pattern of the controls (Mannan and PAA-Le^X, respectively). DC-SIGN also showed a positive binding to the studied glyconanomaterials without a significant difference between **2** and **3**. These data were confirmed by titration studies using increasing concentrations of the tested lectins (ESI,† Fig. S14). Accordingly, langerin showed the capacity to differentiate between the two glyconanomaterials **2** and **3** (ESI,† Fig. S14). Conversely, the unfunctionalized CNC–Au–LA **1** exhibited lower binding to the tested lectins than the glycoconjugates bearing the monosaccharide headgroups (Fig. 2). The mannose receptor (MR) was selected as a third CLR belonging to a different group (group 6),[23] indeed it has a different carbohydrate-recognition-domain organization compared to langerin and DC-SIGN. As reported in Fig. S15 (ESI†), MR showed a weaker binding to the tested nanomaterials compared to langerin and DC-SIGN.

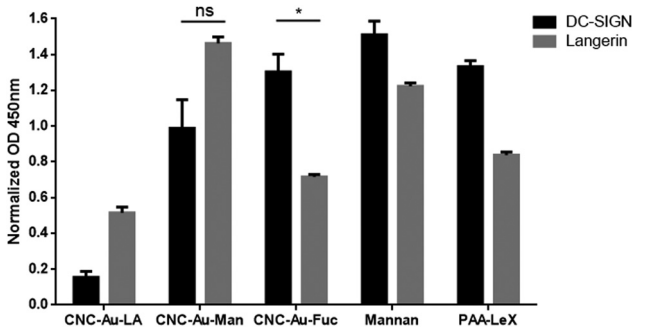

Fig. 2 Binding of CNC–AuNP conjugates **2** and **3** and of the CNC–Au–LA **1** to C-type lectin-Fc constructs of langerin (chimera langerin-Fc lectin)[21] and DC-SIGN (Ig fusion protein, DC-SIGN-Fc),[22] measured by ELISA. Wells were coated with the corresponding glyconanomaterials **1–3** and the binding of lectins-Fc was measured as Optical density (OD) read at 450 nm. Data were normalized against BSA-coated wells used as blocking agent. Bars show the average signal from independent experiments performed in duplicate. Error bars indicate standard deviations of between the mean values from three independent experiments performed in duplicate. One asterisk indicates a p-value < 0.05; ns: not significant.

The results indicate that the glyconanomaterial **2–3** displays the sugar headgroups so that their binding to human carbohydrate-binding receptors is preserved. Overall, the turbidimetry and ELISA assays confirm that the engineered CNC–AuNPs hybrids are suitable glyconanomaterials to study and intervene in glycan–lectin interactions.

Then, according to the ELISA preliminary screening we decided to further investigate the interaction between the CNC–AuNPs conjugates **2** and **3** and CLRs langerin and DC-SIGN by microscopy. In particular, cryo-transmission electron microscopy (cryo-TEM) is a powerful technique for structural biology and it has recently been utilized to determine the three-dimensional structure of relevant (glyco)-proteins and to study structural changes in their native biological environments with a high degree of detail and a sub-nanoscale resolution.[24] This technique also enables direct visualization of glycan–protein interactions, as samples are frozen at cryogenic temperatures that lock specimens in their intact and native state allowing visualization of assembled structures.[25]

In this regard, we sought to investigate the observed interactions between the CNC–AuNPs conjugates **2** and **3** and the chimera lectins langerin and DC-SIGN by cryo-TEM, using TMS as a buffer (20 mM tris(hydroxymethyl)aminomethane (TRIS), 150 mM NaCl, 1 mM $CaCl_2$, 2 mM $MgCl_2$, pH = 8). The CNC–Au–LA **1** was used as a control to assess the role of the sugar headgroups in the recognition. Images of the mixture between CNC–Au–LA **1** and langerin (Fig. 3A) or DC-SIGN (Fig. 3B) in TMS buffer displayed a homogeneous distribution of isolated and non-assembled CNC needles that likewise appear in cryo-TEM images of CNC suspensions.[26]

On the other hand, images of a mixture of CNC–Au–Man **2** (Fig. 3C) or CNC–Au–Fuc **3** (Fig. 3E) and the langerin in TMS buffer indicated the formation of packed networks where CNC nanorods are organized in self-assembled structures. In particular, CNC–Au–Man **2** and langerin form self-assembled architectures which are shaped like bundles of needles (Fig. 3C). Notably, the same mixture in TRIS buffer plus EDTA (4 mM), to remove residual

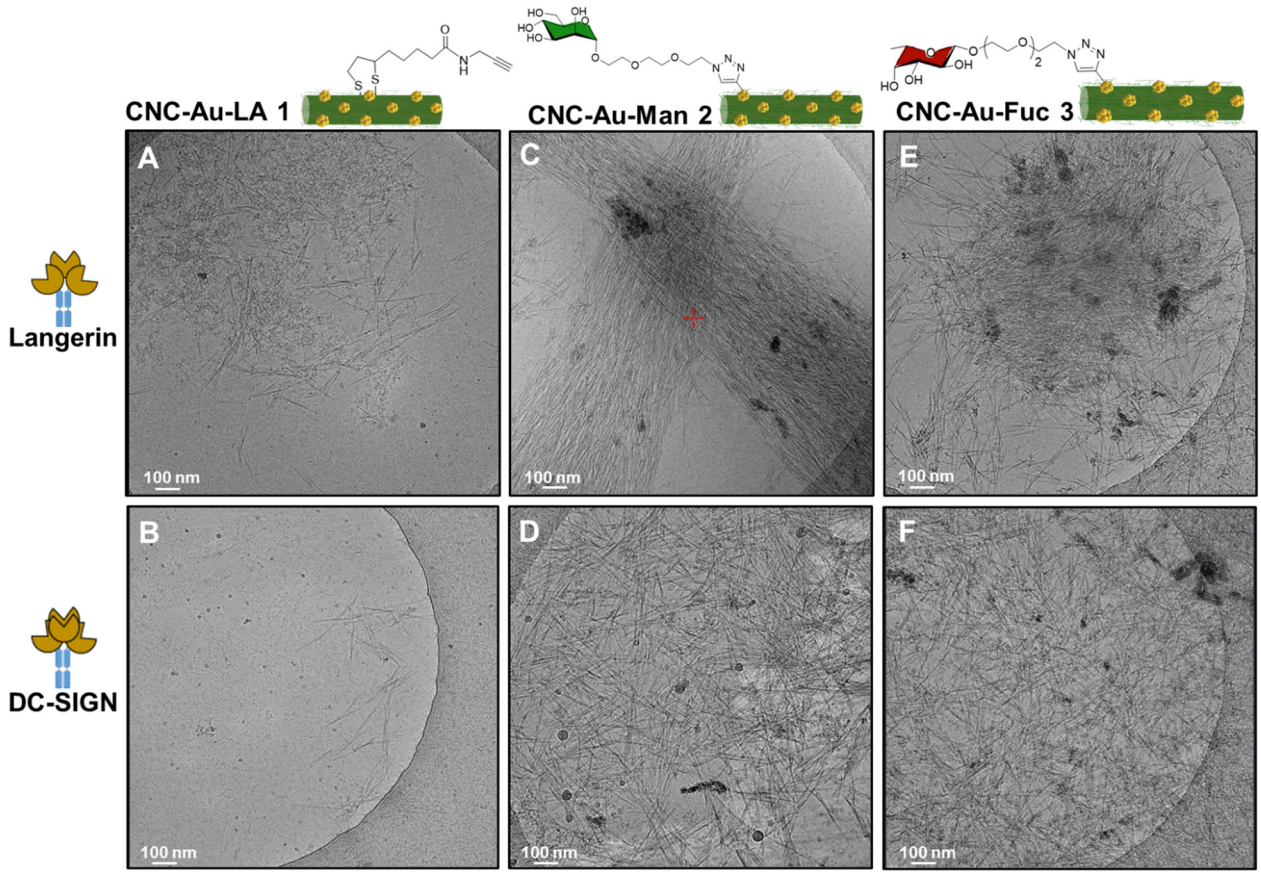

Fig. 3 Cryo-TEM images of the chimera lectins langerin-Fc and DC-SIGN-Fc in TMS treated with a dispersion (0.01% w/w in H_2O) of CNC–Au–LA **1** (A and B), respectively; or CNC–Au–Man **2** (C and D), respectively; or CNC–Au–Fuc **3** (E and F), respectively. Chimera lectins were used at the final concentration of 0.1 mg mL^{-1} (ESI†). Buffer TMS: 20 mM TRIS, 150 mM NaCl, 1.0 mM $CaCl_2$, 2.0 mM $MgCl_2$, pH = 8. Scale bar 100 nm.

Ca^{2+} ions from the stock solution of the lectin, resulted in more disjointed assembled structures as an indication that some interactions were disrupted by the EDTA removal of the Ca^{2+} ions (ESI,† Fig. S16). Conversely, both CNC–AuNPs conjugates **2** and **3** treated with DC-SIGN showed a resemblance in the organization of the assembled structures that resulted in a thick aggregation of needles (Fig. 3D and F).

Conclusion

We demonstrate that CNC–Au–LA **1** is an unprecedented modular glyconanomaterial whose surface can be easily modified with one or two different headgroups by click chemistry. The proper arrangement of CLR-targeting moieties on its surface and the morphological features of the polysaccharide-based glyconanomaterial make our hybrid cellulose nanocrystal–gold nanoparticles a unique multivalent scaffold suitable for displaying multiple copies of sugar headgroups for direct visualization of glycan–lectin interactions by cryogenic microscopy.

Targeting C-type lectins *i.e.* DC-SIGN and langerin has been a long sought-after goal in the design of glyconanomaterials meant for different therapies (anticancer, antimicrobial) or immune modulation.[27] Importantly, receptor-mediated endocytosis with minimal nonspecific uptake enables the selective treatment of immune cells.[27a] Taken together, these findings pave the way for further investigations of CLR-specific antigen delivery applications.

Author contributions

B. R. and F. C. are responsible for conceptualization, funding, acquisition, resources and writing – original draft & review & editing. G. B., G. T., M. A., M. S., P. A., M. M., H. K., G. T., A. G., are responsible for data curation, and investigation. M. M., C. S., J. R., M. M., S. C., I. U., Y. vK., D. B., F. C., B. R. are responsible for formal analysis, methodology, resources and writing – original draft. G. B., M. A., M. M., H. A., G. T., are responsible for validation and visualization. B. R. is responsible for supervision and project administration. All authors approved the final version of the manuscript.

Conflicts of interest

There are no conflicts to declare.

Acknowledgements

G. B., F. C. M. M., and B. R., thank COST Action CA18103 INNOGLY: Innovation with glycans: new frontiers from synthesis to new biological targets. G. B. G. T., M. A., M. S., P. A., G. T., A. G., D. B., C. S., M. M., S. C. and B. R. thank MIUR-Italy (''Progetto Dipartimenti di Eccellenza 2018–2022'', allocated to the Department of Chemistry ''Ugo Schiff''). We acknowledge the Florence Center for Electron Nanoscopy (FloCEN) at the University of Florence. G. B. and B. R. thank Fondazione Umberto Veronesi for supporting the post-doctoral fellowship of G. B. (Grant numbers: 4731, 4451 and 5167). B. R. thanks L'Amore di Matteo Coveri ONLUS for financial support. J. R. acknowledges a grant from MCIN/AEI/10.13039/501100011033 (PID2020-118403GB-I00). I. U. and H. K. thank the Slovenian Research Agency (P1-0060) for financial support.

References

1 (*a*) G. Delepierre, O. M. Vanderfleet, E. Niinivaara, B. Zakani and E. D. Cranston, *Langmuir*, 2021, **37**, 8393–8409; (*b*) D. Trache, A. F. Tarchoun, M. Derradji, T. S. Hamidon, N. Masruchin, N. Brosse and M. H. Hussin, *Front. Chem.*, 2020, **8**, 392.

2 (*a*) S. Dong, A. A. Hirani, K. R. Colacino, Y. W. Lee and M. Roman, *Nano LIFE*, 2012, **02**, 1241006; (*b*) I. Lugoloobi, H. Maniriho, L. Jia, T. Namulinda, X. Shi and Y. Zhao, *J. Controlled Release*, 2021, **336**, 207–232; (*c*) Y. Y. Khine and M. H. Stenzel, *Mater. Horiz.*, 2020, **7**, 1727–1758; (*d*) T. V. Patil, D. K. Patel, S. D. Dutta, K. Ganguly, T. S. Santra and K. T. Lim, *Bioact. Mater.*, 2022, **9**, 566–589.

3 N. Grishkewich, N. Mohammed, J. Tang and K. C. Tam, *Curr. Opin. Colloid Interface Sci.*, 2017, **29**, 32–45.

4 (*a*) M. Zhu, G. Nie, H. Meng, T. Xia, A. Nel and Y. Zhao, *Acc. Chem. Res.*, 2013, **46**, 622–631; (*b*) B. Kang, T. Opatz, K. Landfester and F. R. Wurm, *Chem. Soc. Rev.*, 2015, **44**, 8301–8325.

5 (*a*) S. Eyley and W. Thielemans, *Nanoscale*, 2014, **6**, 7764–7779; (*b*) H. Tao, N. Lavoine, F. Jiang, J. Tang and N. Lin, *Nanoscale Horiz.*, 2020, **5**, 607–627.

6 M. S. Islam, L. Chen, J. Sisler and K. C. Tam, *J. Mater. Chem. B*, 2018, **6**, 864–883.

7 (*a*) J. Van Rie and W. Thielemans, *Nanoscale*, 2017, **9**, 8525–8554; (*b*) O. Ya. Uryupina, V. V. Vysotskii, V. V. Matveev, A. V. Gusel'nikova and V. I. Roldughin, *Colloid J.*, 2011, **73**, 551–556.

8 (*a*) Q. Wei, Y. Su, H. Xin, L. Zhang, J. Ding and X. Chen, *ACS Appl. Mater. Interfaces*, 2021, **13**, 56719–56724; (*b*) S.-J. Richards and M. I. Gibson, *JACS Au*, 2021, **1**, 2089–2099.

9 (*a*) Q. Lu, J. Wu, H. Wang and B. Huang, *Polymers*, 2022, **14**, 1313; (*b*) R. Li, Y. Liu, F. Seidi, C. Deng, F. Liang and H. Xiao, *Adv. Mater. Interfaces*, 2022, **9**, 2101293; (*c*) V. Gabrielli, E. Missale, M. Cattelan, M. F. Pantano and M. Frasconi, *Mater. Today Chem.*, 2022, **24**, 100886.

10 L. Chatwell, A. Holla, B. B. Kaufer and A. Skerra, *Mol. Immunol.*, 2008, **45**, 1981–1994.

11 M. Brust, M. Walker, D. Bethell, D. J. Schiffrin and R. Whyman, *J. Chem. Soc., Chem. Commun.*, 1994, 801–802.

12 M. Zhou, C. Zeng, Y. Chen, S. Zhao, M. Y. Sfeir, M. Zhu and R. Jin, *Nat. Commun.*, 2016, **7**, 1–7.

13 J. Tricomi, M. Cacaci, G. Biagiotti, L. Caselli, L. Niccoli, R. Torelli, A. Gabbani, M. Di Vito, F. Pineider, M. Severi, M. Sanguinetti, E. Menna, M. Lelli, D. Berti, S. Cicchi, F. Bugli and B. Richichi, *Nanoscale*, 2022, **14**, 10190–10199.

14 S. Fedeli, P. Paoli, A. Brandi, L. Venturini, G. Giambastiani, G. Tuci and S. Cicchi, *Chem. – Eur. J.*, 2015, **21**, 15349–15353.

15 J. Zhou, N. Butchosa, H. S. N. Jayawardena, J. Park, Q. Zhou, M. Yan and O. Ramström, *Biomacromolecules*, 2015, **16**, 1426–1432.

16 R. J. Pieters, *Org. Biomol. Chem.*, 2009, **7**, 2013–2025.

17 (*a*) H. Bavireddi and R. Kikkeri, *Analyst*, 2012, **137**, 5123–5127; (*b*) N. Kamiya, M. Tominaga, S. Sato and M. Fujita, *J. Am. Chem. Soc.*, 2007, **129**, 3816–3817; (*c*) P. Babu, S. Sinha and A. Surolia, *Bioconjugate Chem.*, 2007, **18**, 146–151.

18 R. Kikkeri, L. H. Hossain and P. H. Seeberger, *Chem. Commun.*, 2008, 2127.

19 S. Boden, K. G. Wagner, M. Karg and L. Hartmann, *Polymers*, 2017, **9**, 1–27.

20 F. Chiodo, M. Marradi, B. Tefsen, H. Snippe, I. van Die and S. Penadés, *PLoS One*, 2013, **8**, e73027.

21 C. M. Fehres, S. Duinkerken, S. C. Bruijns, H. Kalay, S. J. van Vliet, M. Ambrosini, T. D. de Gruijl, W. W. Unger, J. J. Garcia-Vallejo and Y. van Kooyk, *Cell. Mol. Immunol.*, 2017, **14**, 360–370.

22 T. B. H. Geijtenbeek, G. C. F. van Duijnhoven, S. J. van Vliet, E. Krieger, G. Vriend, C. G. Figdor and Y. van Kooyk, *J. Biol. Chem.*, 2002, **277**, 11314–11320.

23 (*a*) L. Martinez-Pomares, D. Wienke, R. Stillion, E. J. McKenzie, J. N. Arnold, J. Harris, E. McGreal, R. B. Sim, C. M. Isacke and S. Gordon, *Eur. J. Immunol.*, 2006, **36**, 1074–1082; (*b*) K. Drickamer and M. E. Taylor, *Curr. Opin. Struct. Biol.*, 2015, **34**, 26–34.

24 D. Wrapp, N. Wang, K. S. Corbett, J. A. Goldsmith, C.-L. Hsieh, O. Abiona, B. S. Graham and J. S. McLellan, *Science*, 2020, **367**, 1260–1263.

25 (*a*) V. Heine, C. Dey, P. Bojarová, V. Křen and L. Elling, *Biotechnol. Adv.*, 2022, 107928; (*b*) S. Bertuzzi, A. Gimeno, A. Martinez-Castillo, M. G. Lete, S. Delgado, C. Airoldi, M. Rodrigues Tavares, M. Bláhová, P. Chytil, V. Křen, N. G. A. Abrescia, A. Ardá, P. Bojarová and J. Jiménez-Barbero, *Int. J. Mol. Sci.*, 2021, **22**, 6000; (*c*) W. Qi, Y. Zhang, Z. Kochovski, J. Wang, Y. Lu, G. Chen and M. Jiang, *Nano Res.*, 2018, **11**, 5566–5572.

26 T. Abitbol, E. Kloser and D. G. Gray, *Cellulose*, 2013, **20**, 785–794.

27 (*a*) M. Anderluh, F. Berti, A. Bzducha-Wróbel, F. Chiodo, C. Colombo, F. Compostella, K. Durlik, X. Ferhati, R. Holmdahl, D. Jovanovic, W. Kaca, L. Lay, M. Marinovic-Cincovic, M. Marradi, M. Ozil, L. Polito, J. J. Reina-Martin, C. A. Reis, R. Sackstein, A. Silipo, U. Švajger, O. Vaněk,

F. Yamamoto, B. Richichi and S. J. Vliet, *FEBS J.*, 2021, **288**, 4746–4772; (*b*) M. Anderluh, F. Berti, A. Bzducha-Wróbel, F. Chiodo, C. Colombo, F. Compostella, K. Durlik, X. Ferhati, R. Holmdahl, D. Jovanovic, W. Kaca, L. Lay, M. Marinovic-Cincovic, M. Marradi, M. Ozil, L. Polito, J. J. Reina, C. A. Reis, R. Sackstein, A. Silipo, U. Švajger, O. Vaněk, F. Yamamoto, B. Richichi and S. J. Vliet, *FEBS J.*, 2021, **289**, 4251–4303.

